Numerical Modelling of Epidermal Wound Healing

E. Javierre, F.J. Vermolen, C. Vuik, and S. van der Zwaag

Abstract A coupling between wound closure by cell migration and angiogenesis is presented here to model healing of epidermal wounds. The closure of the wound is modelled as a moving interface around which a local grid refinement is applied. The numerical solution combines finite element and finite difference methods to solve the coupled diffusion-reaction equations governing the physiological problem and the hyperbolic equations governing the motion of the interface.

We discuss the accuracy and workload of our numerical model. Furthermore, we illustrate that, under certain circumstances, the healing process may be stopped after initiation.

1 Introduction

Wound healing proceeds by a succession of chemical and mechanical processes: removal of infectious matter by phagocytes, cell mitosis and cell migration to close the wound, extracellular matrix synthesis, reparation of the vascular network (angiogenesis) and, in deeper wounds, reduction of the wound size due to stresses on the tissue (wound contraction). Most of these processes are triggered by the presence or lack of certain growth factors, and are terminated due to a negative feedback mechanism.

E. Javierre and S. van der Zwaag
Fundamentals of Advanced Materials, Faculty of Aerospace Engineering, Delft University of Technology, Kluyverweg 1, 2629 HS Delft, The Netherlands, e-mail: [E.JavierrePerez, S.vanderZwaag]@tudelft.nl

F.J. Vermolen and C. Vuik
Delft Institute of Applied Mathematics, Faculty of Electrical Engineering, Mathematics and Computer Science, Delft University of Technology, Mekelweg 4, 2628 CD Delft, The Netherlands e-mail: [F.J.Vermolen, C.Vuik]@tudelft.nl

Mathematical models for wound healing normally consider only one isolated process. For example, wound closure is studied in [2, 4, 13, 14], angiogenesis in [1, 5, 8] and wound contraction in [9, 10]. However, it is well known that these processes overlap and affect one another. In the present work, we couple wound closure due to cell migration with angiogenesis. In contrast to the discrete models related to cell population dynamics [1, 3], wound closure is modelled here as a closed curve (the wound edge) moving into the wound in the course of time. Hence, the model presented here consists of a number of coupled diffusion-reactions with a moving interface.

The remainder of this paper is organized as follows. The mathematical model is given in Section 2. Subsequently, the computational approach is described in Section 3. Section 4 gives some numerical results that show the potential of the model, and the conclusions are given in Section 5.

2 The Mathematical Model

We combine the models of wound closure due to Arnold and Adam [2] and the model of angiogenesis due to Maggelakis [8] to obtain a new model that couples both processes. In the first model, the closure of the wound is triggered by the production of an epidermic growth factor (EGF) that determines the cell mitosis and motility. Furthermore, the wound edge is identified as the advancing front of cells closing the wound, and the closure rate depends on the curvature of the wound according to a phenomenological relation. In the latter model, the capillaries supply the wound with the necessary oxygen and nutrients needed in the healing process. The lack of oxygen at the wound site stimulates the appearance of macrophages at the wound surface which produce macrophage-derived growth factors (MDGFs) that trigger the regeneration of the vascular system.

Our coupling of both models is based on the following hypotheses [6]: (H1) the production of EGFs only takes place if there is enough oxygen to support it, (H2) the excess of oxygen enhances the production of EGFs, and (H3) the equilibrium capillary density is larger under the wound than anywhere else. Consequently, (H1) delays the actual healing and (H2)-(H3) intend to speed up the healing process after the incubation period.

We consider the distribution of the oxygen concentration u_1, the MDGF concentration u_2, the capillary density u_3 and the EGF concentration u_4 over the computational domain Ω, which is two-dimensional (since the thickness of the epidermis is very small compared to the wound dimensions) and Lipschitz. Moreover, Ω consists of the wounded tissue Ω_w, the active layer Ω_{al} surrounding the wound where the EGFs are being produced, and the outer tissue Ω_{ot}. The wound edge is denoted by Γ. From a mass balance argument we obtain the governing equations describing the transport, production and decay of these quantities:

$$\frac{\partial u_1}{\partial t} = D_1 \Delta u_1 + \lambda_{3,1} u_3 - \lambda_{1,1} u_1, \tag{1}$$

$$\frac{\partial u_2}{\partial t} = D_2 \Delta u_2 + \lambda_{1,2} Q(u_1) - \lambda_{2,2} u_2, \tag{2}$$

$$\frac{\partial u_3}{\partial t} = D_3 \Delta u_3 + \lambda_{3,2} u_2 u_3 \left(1 - \frac{u_3}{u_3^{eq}(1+qH(\phi))}\right), \tag{3}$$

$$\frac{\partial u_4}{\partial t} = D_4 \Delta u_4 - \lambda_{4,4} u_4 + P f(\mathbf{x}, t, u_1, p), \tag{4}$$

where D_i denote the diffusion coefficients, $\lambda_{i,j}$ the production/decay rates, u_i^{eq} the values of the undamaged state (which is an equilibrium state), P the production rate of EGFs and H the heaviside function. Moreover, Q denotes the function describing the production of MDGF when the levels of oxygen are low and f stands for the production of EGF inside the active layer, which, respectively, are defined as

$$Q(u_1) = \begin{cases} 1 - \frac{u_1}{u_1^{\theta_2}}, & \text{if } u_1 < u_1^{\theta_2}, \\ 0, & \text{otherwise,} \end{cases} \tag{5}$$

and

$$f(\mathbf{x}, t, u_1, p) = \begin{cases} 1 + p\frac{u_1}{u_1^{\theta_4}}, & \text{if } u_1 \geq u_1^{\theta_4} \text{ and } \mathbf{x} \in \Omega_{al}(t), \\ 0, & \text{otherwise.} \end{cases} \tag{6}$$

Equations (1)-(4) are supplemented with homogeneous Neumann boundary conditions and the following initial conditions:

$$u_i(\cdot, 0) = \begin{cases} 0, & \text{in } \Omega_w(0), \\ u_i^{und}, & \text{otherwise,} \end{cases} \qquad \text{and} \qquad u_j(\cdot, 0) = 0 \text{ in } \Omega, \tag{7}$$

where $i = 1, 3$, $j = 2, 4$ and u_i^{und} denote the (equilibrium) undamaged levels. The parameters p and q are used to describe the influence of oxygen in the production of EGFs and to enhance the capillary regeneration inside the wound respectively, whereas $u_1^{\theta_2}$ and $u_1^{\theta_4}$ denote the oxygen concentration below which MDGFs are produced and EGFs are not produced. Finally, the wound will move towards closure only if the concentration of EGF exceeds a certain threshold value $u_4^{\theta_4}$. Hence, normal velocity v_n of the wound edge is given by

$$v_n(\mathbf{x}, t) = \big(\alpha + \beta \kappa(\mathbf{x}, t)\big) H\big(u_4(\mathbf{x}, t) - u_4^{\theta^4}\big) \quad \text{for } \mathbf{x} \in \Gamma(t), \tag{8}$$

where the normal vector $\mathbf{n}$ points into the wound, α, β are non-negative and κ denotes the local curvature.

Note that each time step we need to find the wound edge in order to properly compute the concentrations u_i, i =1, ..., 4. Hence, we are dealing with a moving boundary problem.

3 The Computational Approach

The solution of equations (1)–(4) is computed using a finite element method with piecewise linear basis functions. The time integration of the governing equations is carried out with an Implicit-Explicit Euler method, where only the nonlinear reaction terms are treated explicitly, and Newton-Cotes integration rules are applied in the calculation of the element matrices and vectors. Further, we have to deal with a moving interface and with a sharp (discontinuous) change of the production of the EGF across the wound edge. In order to track the front position in a fashion that allows us handling changes in the wound geometry easily and to obtain a quick identification of the subparts of the computational domain we use the Level Set Method [11]. Furthermore, we apply an adaptive mesh technique in the vicinity of the wound edge. In this way we recover some of the accuracy lost due to the discontinuous production of EGF and have a higher resolution in the region where the motion of the interface is computed. We refer the interested reader to [7] to find the technical details of the algorithm.

3.1 The Level Set Method for Tracking the Wound Edge

In the level set method, the wound edge is defined as the zero level set of a continuous scalar function ϕ:

$$\mathbf{x} \in \Gamma(t) \iff \phi(\mathbf{x},t) = 0, \quad \forall t \geq 0. \tag{9}$$

Furthermore, the so-called level set function ϕ is initialized and subsequently maintained as a signed distance function ($||\nabla\phi|| = 1$), being positive inside the wound and negative outside. To achieve this, we apply the Fast Marching Method [12] to solve the Eikonal equation $||\nabla\phi|| = 1$ each time step. Hence, if ϕ is a distance function, the domain of computation Ω is parameterized as follows:

$$\Omega_w(t) = \{\mathbf{x} \in \Omega \mid 0 < \phi(\mathbf{x},t)\}, \tag{10}$$

$$\Omega_{al}(t) = \{\mathbf{x} \in \Omega \mid -\delta(\mathbf{x},t) < \phi(\mathbf{x},t) < 0\}, \tag{11}$$

$$\Omega_{ot}(t) = \{\mathbf{x} \in \Omega \mid \phi(\mathbf{x},t) < -\delta(\mathbf{x},t)\}, \tag{12}$$

where δ denotes the thickness of the active layer. The motion of the wound edge is then followed by the advection of the level set function:

$$\frac{\partial\phi}{\partial t} + \mathbf{v}\cdot\nabla\phi = 0, \tag{13}$$

where the advection field $\mathbf{v}$ denotes any continuous extension of the front velocity (8). In this work we advect v_n from the interface position in the normal direction [7].

3.2 The Adaptive Mesh Strategy

We choose as a fixed basis mesh a structured triangulation like the one presented in Fig. 1 (left). At each time step, we refine the elements within a certain distance *dist* from the interface, and the elements adjacent to them in order to preserve mesh consistency. Each edge marked to be refined will be subdivided into equally sized sub-edges that will define the new elements, as depicted in Fig. 1 (center). In order to prevent ill-shaped elements, we will limit ourselves to refinement ratios equal to 2 or 3 (*i.e.* each marked edge will be divided into 2 or 3 sub-edges respectively). The refined mesh inherits the structure of the basis mesh, presenting a refined Cartesian band within the refined region and a coarse Cartesian grid outside, see Fig. 1 (right). We take benefit of this structure as finite difference schemes are applied to the hyperbolic equations (such that the velocity extension and the advection and the reinitialization of the level set function) inherited from the level set formulation, and hence avoid the implementation of stabilization techniques in the finite element approximations.

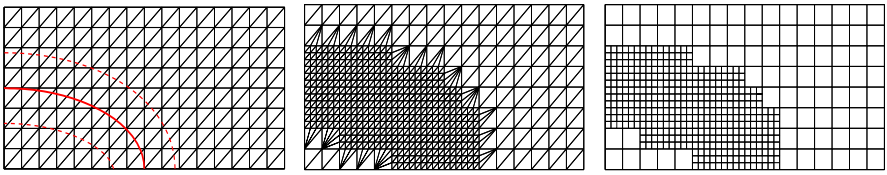

Fig. 1 Left: fixed base FE mesh with the interface position $\phi = 0$ (solid curve) and the contours $\phi = \pm dist$ (dashed curves). The elements within these contours are to be refined. Center: refined FE mesh. Right: the nested Cartesian grids.

4 Numerical Results

4.1 Accuracy and Workload of the Computational Method

The accuracy of the adaptive grid strategy is evaluated here by measuring the relative error of the epidermic growth factor concentration, for the fully uncoupled model, after an incubation period of 45 minutes. The L^2 norm of the relative error in the EGF concentration is presented in the third column of Table 1. The closure of the wound has not been included in this test, and the analytical solution has been obtained for a circular wound after applying separation of variables and expressing the production function f as a series expansion of the eigenfunctions of the homogeneous problem. The numerical results show that, despite the fact that we use linear elements (P_1) in our finite element approximation, the numerical solution is only first order accurate because of the discontinuous production of EGFs. However, it

is worth noting that we recover the accuracy for the fixed basis mesh with double number of gridnodes in each dimension if the refinement ratio is set equal to 2 in the coarse grid, and a bit more when it is set equal to 3.

The following columns of Table 1 present the number of elements and the arrangement of the nodal points inside and outside the refined band for several refinement ratios, as well as for the unrefined mesh. The CPU-times employed in the reinitialization of the level set function inside and outside the refined Cartesian band are given in the seventh and eighth columns. The number of elements gives us an estimate of the workload needed to build the system of equations of the discretized problem (*i.e.* updating the right hand side vectors). Since we use the Fast Marching Method, the workload of the reinitialization step is $\mathcal{O}(n \log n)$, where n denotes the number of nodes in the reinitialization region. The numerical results show that the workload sharply increases inside the refined band when the number of nodes increases. Furthermore, the reinitialization of ϕ outside the band cannot be avoided because it is necessary to accurately identify the active layer each time step. Use of a fine fixed basis mesh has been proven to increase the CPU-time per time step. Instead, we suggest to use coarser fixed base grids with higher levels of refinement, since then the workload of the reinitialization steps (inside and outside the refined band) are well balanced and the accuracy is preserved, as can be observed by comparison of the results for N=161 without local refinement and for N=81 with refinement ratio equal to 3.

Table 1 Performance of the computational method. N denotes the number of nodes per Cartesian direction and − indicates that the fixed basis mesh is not refined. The refinement distance *dist* is kept proportional to the mesh width.

N	Ref. ratio	L^2 error	#elements	#nodes inside band	#nodes outside band	Reinitialization inside band	Reinitialization outside band
	-	$3.03 \cdot 10^{-1}$	800	80	361	0.05s	0.27s
21	2	$1.51 \cdot 10^{-1}$	1186	277	361	0.19s	0.26s
	3	$1.31 \cdot 10^{-1}$	1808	592	361	0.45s	0.26s
	-	$1.61 \cdot 10^{-1}$	3200	156	1525	0.11s	1.21s
41	2	$7.55 \cdot 10^{-2}$	3978	549	1525	0.45s	1.19s
	3	$6.09 \cdot 10^{-2}$	5232	1180	1525	1.03s	1.20s
	-	$8.07 \cdot 10^{-2}$	12800	308	6353	0.27s	6.30s
81	2	$3.75 \cdot 10^{-2}$	14362	1093	6253	1.10s	6.28s
	3	$2.87 \cdot 10^{-2}$	16880	2356	6253	2.55s	6.25s
	-	$4.11 \cdot 10^{-2}$	51200	598	25323	0.69s	46.52s
161	2	$2.15 \cdot 10^{-2}$	54294	2157	25323	2.89s	45.75s
	3	$1.52 \cdot 10^{-2}$	59296	4663	25323	6.87s	45.60s

4.2 Healing of an Elliptical Wound

The healing of an elliptical wound is simulated in this section. The solutions u_i ($i = 1,\ldots,4$) after 5% of the wound has healed are plotted in Fig. 2. These plots clearly illustrate the lack of oxygen at the wound site and the resulting high concentration of macrophage-derived growth factors. The plot of the capillary density distinctly shows the role of wound geometry on the healing process. The influence of wound geometry has already been studied in detail for the closure model in [7], and it will be analysed in depth for the coupled model in a future study. Finally, the epidermic growth factor concentration profile shows the location of the active layer. The small wiggles observed in the EGF concentration are believed to be a numerical artifact related to the threshold oxygen level imposed on the production of the EGF.

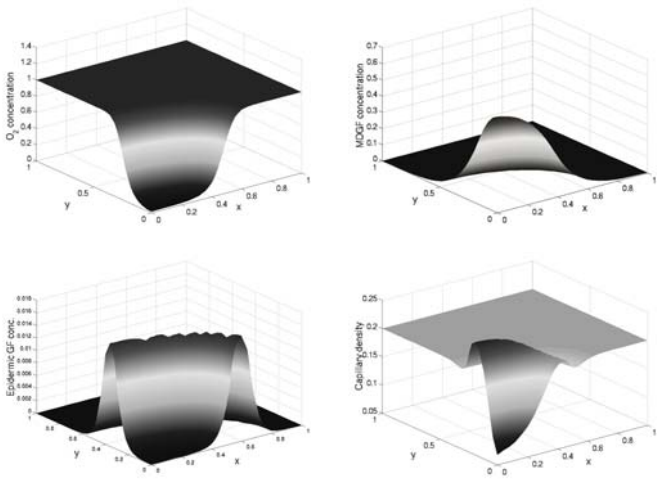

Fig. 2 Oxygen concentration (top left), MDGF concentration (top right), EGF concentration (bottom left) and capillary density (bottom right) for elliptical wound after 5% of it has healed.

4.3 The Revised Critical Size Defect

Arnold and Adam [2] use the EGF model to predict the Critical Size Defect (CSD) of a wound, which is defined as the smallest wound that does not heal during the life time of the animal. Since they do not include the time evolution of the wound, their prediction only allows to elucidate the minimal size of the (circular) wound for which some healing must be expected. However, starting the healing is no guarantee of completing it successfully. Our simulations revealed that there are cases in which the healing process halts prematurely after healing has started. This was observed

when the closure rate was excessively slow or the active layer was unable to produce the necessary EGFs.

5 Conclusions

A coupling between wound closure and angiogenesis is presented in this work. The closure of the wound is modelled as a moving interface problem, where the interface is identified with the advancing front of epidermal cells and the Level Set Method is applied to track its position in time. A finite element method is used to solve the governing equations and an adaptive mesh algorithm is implemented because of the discontinuous production of EGFs across the edges of the active layer. The numerical results show that the refinement around the wound edge allows us to recover some of the accuracy lost due aforementioned discontinuity. Furthermore, the width of the fixed basis mesh and the refinement ratio must be chosen in a proper way to bring the workload per time step and the accuracy of the results into balance.

References

1. Anderson, A., Chaplain, M.: Continuous and discrete mathematical models of tumor-induced angiogenesis. Bulletin of Mathematical Biology **60**, 857–900 (1998)
2. Arnold, J.S., Adam, J.A.: A simplified model of wound healing. II. The critical size defect in two dimensions. Math. Comput. Modelling **30**(11-12), 47–60 (1999)
3. Cai, A.Q., Landman, K.A., Hughes, B.D.: Multi-scale modeling of a wound-healing cell migration assay. J. Theoret. Biol. **245**(3), 576–594 (2007)
4. Gaffney, E., Maini, P., Sherratt, J., Tuft, S.: The mathematical modelling of cell kinetics in corneal epithelial wound healing. Journal of Theoretical Biology **197**, 15–40 (1999)
5. Gaffney, E.A., Pugh, K., Maini, P.K., Arnold, F.: Investigating a simple model of cutaneous wound healing angiogenesis. J. Math. Biol. **45**(4), 337–374 (2002)
6. Gordillo, G., Sen, C.: Revisiting the essential role of oxygen in wound healing. The American Journal of Surgery **186**, 259–263 (2003)
7. Javierre, E., Vermolen, F., Vuik, C., Zwaag, S.v.d.: A Mathematical Approach to Epidermal Wound Healing: Model Analysis and Computer Simulations. Tech. Rep. 07-14, Department of Applied Mathematical Analysis, Delft University of Technology (2007)
8. Maggelakis, S.: A mathematical model of tissue replacement during epidermal wound healing. Applied Mathematical Modelling **27**, 189–196 (2003)
9. Murray, J.D.: Mathematical biology. II, *Interdisciplinary Applied Mathematics*, vol. 18, third edn. Springer-Verlag, New York (2003). Spatial models and biomedical applications
10. Olsen, L., Sherrat, J., Maini, P.: A mechanochemical model for adult dermal wound contraction and the permanence of the contracted tissue displacement profile. Journal of Theoretical Biology **177**, 113–128 (1995)
11. Osher, S., Sethian, J.A.: Fronts propagating with curvature-dependent speed: algorithms based on Hamilton-Jacobi formulations. J. Comput. Phys. **79**(1), 12–49 (1988)
12. Sethian, J.A.: Fast marching methods. SIAM Rev. **41**(2), 199–235 (1999)
13. Sherratt, J., Murray, J.: Epidermal wound healing: the clinical implications of a simple mathematical model. Cell Transplantation **1**, 365–371 (1992)
14. Vermolen, F., van Baaren, E., Adam, J.: A simplified model for growth factor induced healing of wounds. Mathematical and Computer Modelling **44**, 887–898 (2006)